Scientia Iranica B (2023) 30(5), 1595–1611

Sharif University of Technology
Scientia Iranica
Transactions B: Mechanical Engineering
http://scientiairanica.sharif.edu

Research Note

Dynamic modeling of the extended mobile robot: Composed N parallel axles, suspension system, and wheels slippage

M. Habibnejad Korayem*, S. Fathollahi Dehkordi, and M. Aghajari

Robotics Research Laboratory, Center of Excellence in Experimental Solid Mechanics and Dynamics, School of Mechanical Engineering, Iran University of Science and Technology, Tehran, Iran.

Received 3 September 2020; received in revised form 7 July 2022; accepted 9 May 2023

KEYWORDS
N-parallel axle's mobile robot;
Wheel's slips;
Platform suspension system;
Euler-Lagrange formulation.

Abstract. In this study, the new mobile robot structure with N parallel axles was designed and developed, as well as its motion equations derived. It uses several parallel axes, which increase its mobility at different surface conditions compared to similar ones. The number of parallel axes in such robotic systems makes studies of the effect of slip mandatory due to the increase in the wheels' contact area. These effects make a difference in the mobile robot kinematic constraints equations. On the other hand, added parallel axels prepare the capability for motion on rough and uneven surfaces. But the mobile platform requires a suspension system to reduce the effects of oscillations due to the floor. Finally, the dynamics model of a mobile robot obtains by considering the effect of wheels' slips, suspension, and parallel axles using Lagrange equations. The concluded model is simulated for a two-axis mobile robot with four wheels in different surface conditions. It can be seen that the deviation of the robot is eminent, besides that the wheel's slips affect the system performance based on the floor conditions. Consequently, the robot deviation on ice is less than that on loose gravel, while the mentioned deviation on loose gravel is twice.

1. Introduction

Mobile robots have become widely used in farming, agriculture research, and, in particular, rescue operations. Considering the research performed in this field, it can be concluded that the ideal road assumption can lead to system errors during motion. When a mobile robot is used to collect farm field data by the vision and high-tech sensors, the road roughness makes noise and undesirable oscillation on the resulting signal. Consequently, the robot's convenient motion has a profound effect on the performance of the system. To address the mentioned problem, the present study proposes the N-axis wheeled mobile robot with an updated suspension system. The proposed system has several applications beyond just road conditions, and it can also be used for discovery operations, etc.

The amounts of slip and rolling of wheels are mainly caused by the traction force exerted from the surface to the robot during the motion of the mobile

*. *Corresponding author.*
E-mail address: Hkorayem@iust.ac.ir (M. Habibnejad Korayem)

doi: 10.24200/sci.2023.56722.4874

robots, which can affect the robot's motion and its expected position [1,2]. Consequently, it is possible that all these factors exerted an effect on the robot's motion and different surfaces [3,4]. The calculation of displacement caused by the longitudinal and lateral slip of the robot platform determines the exact robot position [5]. As a result, the accurate position of the moving robot can be obtained according to a reference coordinate system by summing up the values of a longitudinal and lateral slip of the robot platform with the values of longitudinal and transverse displacements of a mobile base [6–8]. On the other hand, considering the exact dynamic equations of electric motors used as actuators in robot wheels can enhance the robot's performance and approach the robot's actual and calculated position. To increase the accuracy of wheel motors, they can be simulated as flexible joints [9]. Another issue that might arise during robot motion is the shocks exerted on the robot base from wheels or the friction between the surface and wheels, possibly changing the direction of robot motion or ending in losing a proportion of torque applied to wheels. To prevent the exertion of such shocks, one can utilize a spring and damper on each wheel [10].

On the other hand, depending on the choice of motion equations derivation method, including Newton-Euler [11], Euler-Lagrange [12], and Gibbs-Appell [13], different approaches exist for choosing the system generalized coordinates. For deriving the motion equations of this type of mobile robot, the effects of the longitudinal and lateral slip in active wheels is an important matter which is considered such that Alipour and Moosavian [14] used pneumatic wheels and dug-off friction model to describe the longitudinal and lateral slip forces.

In some cases, due to the limited performance of a robot with two actuating wheels, it is necessary to use a mobile robot with more active wheels, the most common type of which is the four-wheeled mobile robot [15]. In this case, the probability of using the mobile robot in different environments whose surfaces generate longitudinal and lateral slip is greater [16], or in addition, to slip in wheels, the contact conditions between wheel and ground have been considered in the form of friction coefficient [17]. This subject has been investigated by a number of researchers in different frameworks, among which the longitudinal and lateral slip for two wheels, four wheels [18,19], six wheels [20], and eight wheels [21] can be mentioned. To this end, a mobile robot with non-holonomic constraints [22,23] and several actuating axles is utilized. In this case, in addition to the effect of slip [24] and damping owing to the existence of height difference and surfaces through which the robot passes, a spring-damper system is used to prevent surface shocks [25]. On the one hand, compared to previous studies, the system generalized coordinates should be changed, and the amount of computational complexity increased. On the other hand, an accurate model of robot behavior can be obtained by considering the effect of platform damping as well as wheel slippage [26]. An exact dynamic model for the motors used in the joints of the wheels to obtain more accurate motion equations for the system. Future research will use these equations to control the robot using Runge-Kutta-based [27] solution techniques.

This study investigates the motion equations of an extended mobile robot with N parallel wheels' axles. In addition, the effects of longitudinal and lateral wheel slips have been considered. As mentioned, this improved model provides the exact position of the robot during the path. Besides that, the model of the wheel's motor is considered similar to the manipulator's flexible joint. It causes the concluded dynamic model to properly calculate the loss of inputted torque in the wheel's motor joint. Additionally, a suspension system composed of two springs and a damper was set up on each wheel to reduce the platform fluctuations. A particle has been designed to connect each parallel spring-damper pair to another one. These springs and dampers can be utilized by considering different coefficients of stiffness and friction. By completing the required improvements in model promotion, the motion equations of an extended wheeled mobile robot with the multi-parallel axes, suspension system on each of its wheels, and assuming the wheel's slip and motor's flexibility are derived. Previous studies have also focused more on the robot base. But this research focuses on robot wheels and their high degrees of freedom. Also, choosing the type of robot wheels and considering different coefficients for them has caused the need to study the robot movement at different levels. Consequently, the concluded equations are simulated for a four-wheeled mobile robot by considering backlash, flexibility, and friction. This simulation is evaluated at four different stages by weighing various traction forces. Moreover, the case in which no suspension system is installed on the robot wheels is also demonstrated.

The rest of this paper is structured as follows. Section 2 represents the kinematics model of the robot. In section 3, the dynamic equations of the N-axis mobile robot are developed. Section 4 includes the simulation performed for evaluating the resulting motion equations.

2. Kinematics of a mobile platform with N parallel axles

In this section, the kinematics of the mobile platform with N parallel axles is investigated. Taking into account the effects of longitudinal and lateral slip, backlash, and resilience as well as friction in

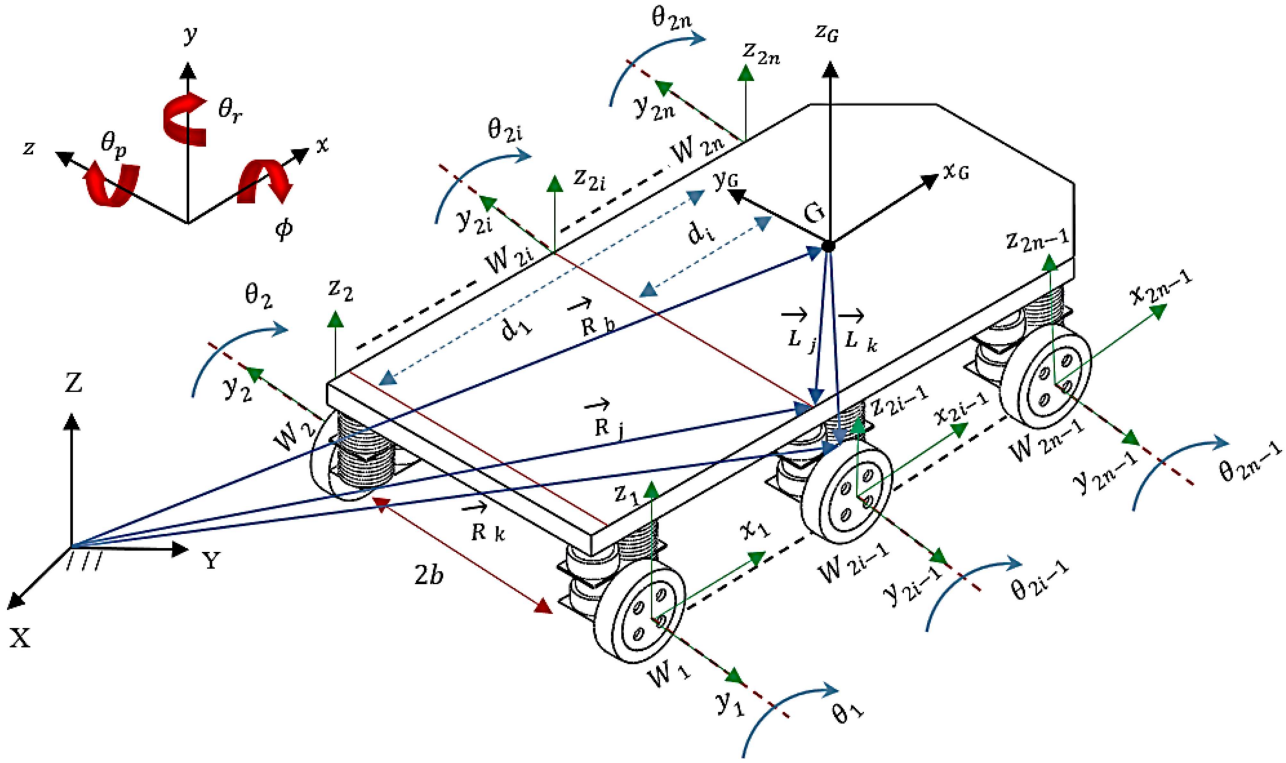

Figure 1. A mobile robot with N parallel axles and $2n$ differential wheels.

the robot wheels, the system variables are chosen as $\mathbf{S} = [\rho_1 \ \rho_2 \ \ldots \ \rho_{2n} \ \eta_1 \ \eta_2 \ \ldots \ \eta_{2n}]$. This selection is based on decomposing the slip vector, where ρ and η represent the longitudinal and lateral slip of the wheels, respectively. According to the explained assumptions for absorbing the shocks of wheels and preventing them from being transferred to the base's connections, two springs and two dampers are considered on each wheel. This setup prevents the wheel displacement from being transferred to the base, whose displacement values are shown by δ which is defined with respect to other generalized coordinates. Consequently, the vector of system generalized coordinates is shown to be:

$$\mathbf{\Theta} = [\mathbf{R}_b^T \mathbf{\Omega}_b^T \eta_1 \ldots \eta_{2n} \rho_1 \ldots \rho_{2n} \theta_1 \ldots \theta_{2n} \theta_{m1} \cdots \theta_{m2n}]^T, \quad (1)$$

where $\mathbf{R}_b^T$ and $\mathbf{\Omega}_b^T$ represent the position of the robot center of mass (point $\boldsymbol{G}$) and Euler angles, respectively. Each of these can also be presented as Eq. (2). Moreover, θ and θ_m in Eq. (1) are the exerted angles (backlash) to the wheels and motors, respectively.

$$\mathbf{R}_b = (x_G, y_G, z_G)^T, \qquad \mathbf{\Omega}_b = (\varphi, \theta_r, \theta_p)^T, \quad (2)$$

where x_G, y_G, z_G determine the position of the base center of mass with respect to the axis of reference coordinate system xyz, and $\theta_r, \theta_p, \varphi$ are, respectively, the yaw, pitch, and roll angles. The location of each point of the robot in the moving or stationary coordinates placed on the robot is depicted in Figure 1.

3. Dynamics of a mobile platform with N parallel axles

In this section, using the Euler-Lagrange formulation, the kinetic energy, Rayleigh dissipation function, and potential energy of the N-axle mobile robot are obtained, based on which the equations of motion are derived. In general, for a robot platform with N parallel axles, the performance of wheels can be placed such that they possess lateral motion in addition to longitudinal motion. Here, in the first step, for a better understanding of the longitudinal and lateral slip of the ith wheel of the robot, two different instances of robot motion are displayed in Figure 2.

Using Eq. (2), the constraint equations for each robot wheel can be expressed as Eq. (3). It is also assumed that the wheel has no longitudinal motion relative to the body:

$$\begin{aligned} &\dot{\rho}_j \cos(\gamma_i) = \dot{x}_G \cos\varphi + \dot{y}_G \sin\varphi + b\dot{\varphi} \\ &\quad j = 1, 3, 5, \ldots, 2n-1 \qquad i = 1, 2, \ldots, n, \\ &\dot{\rho}_k \cos(\gamma_i) = \dot{x}_G \cos\varphi + \dot{y}_G \sin\varphi - b\dot{\varphi} \\ &\quad k = 2, 4, 6, \ldots, 2n \qquad i = 1, 2, \ldots, n. \end{aligned} \quad (3)$$

Upon the deletion of the left-hand side of constraint equations in Eq. (3), the equations change to the form of a simple robot without longitudinal and lateral slips where $\dot{\rho}_i = r\dot{\theta}_i - \dot{\zeta}_i$. For lateral constraints, a similar

$$\mathbf{\Lambda}(\mathbf{\Theta}) = \begin{bmatrix} \cos\varphi & \sin\varphi & 0 & b_1 & 0 & 0 & 0 & \cdots & 0 & -1 & \cdots & -1 & 0 & \cdots & 0 & 0 & \cdots & 0 \\ \cos\varphi & \sin\varphi & 0 & -b_1 & 0 & 0 & 0 & \cdots & 0 & -1 & \cdots & -1 & 0 & \cdots & 0 & 0 & \cdots & 0 \\ \vdots & \vdots & \vdots & \vdots & \vdots & \vdots & \vdots & \vdots & \vdots & \vdots & \vdots & \vdots & \vdots & \vdots & \vdots & \vdots & \vdots & \vdots \\ \cos\varphi & \sin\varphi & 0 & b_n & 0 & 0 & 0 & \cdots & 0 & -1 & \cdots & -1 & 0 & \cdots & 0 & 0 & \cdots & 0 \\ \cos\varphi & \sin\varphi & 0 & -b_n & 0 & 0 & 0 & \cdots & 0 & -1 & \cdots & -1 & 0 & \cdots & 0 & 0 & \cdots & 0 \\ -\sin\varphi & \cos\varphi & 0 & -d_1 & 0 & 0 & -1 & \cdots & -1 & & & & & & & & & \\ \vdots & \vdots & \vdots & \vdots & \vdots & \vdots & \vdots & \vdots & \vdots & & & & & 0_{n\times n} & & & \\ -\sin\varphi & \cos\varphi & 0 & -d_n & 0 & 0 & -1 & \cdots & -1 & & & & & & & & & \end{bmatrix}_{n\times n} \tag{5}$$

where,

$$\dot{\mathbf{\Theta}} = [\dot{\mathbf{R}}_b^T \quad \dot{\mathbf{\Omega}}_b^T \quad \dot{\eta}_1 \quad \dots \quad \dot{\eta}_{2n} \quad \dot{\rho}_1 \quad \dots \quad \dot{\rho}_{2n} \quad \dot{\theta}_1 \quad \dots \quad \dot{\theta}_{2n} \quad \dot{\theta}_{m1} \quad \dots \quad \dot{\theta}_{m2n}]^T. \tag{6}$$

Box I

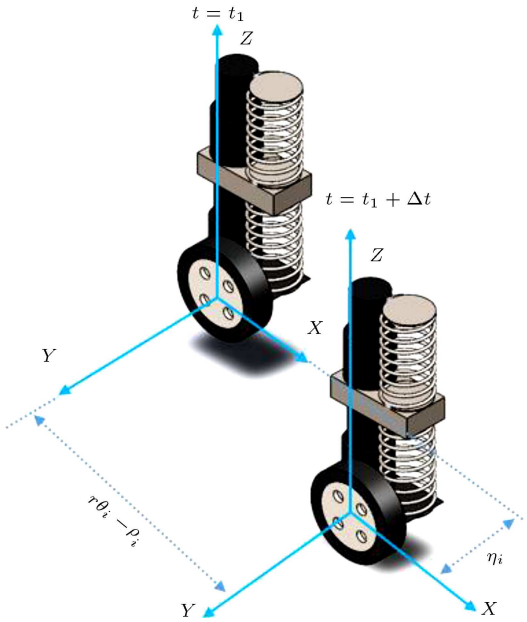

Figure 2. Longitudinal and lateral slip of ith wheel at the moments t_1 and $t_1 + \Delta t$.

approach to that of longitudinal constraints is used with the exception that if the base center of mass is ahead of the wheel axis, the distance from it to the mass center (d_i) is taken as positive. If the wheel axis is ahead of the center of mass, the value of d_i is considered to be negative. Consequently, the lateral constraint equations for each wheel are written as:

$$\dot{\eta}_i \cos(\gamma_i) = \dot{y}_G \cos\phi - \dot{x}_G \sin\phi - d_i\dot{\phi}$$
$$i = 1, ..., 2n, \tag{4}$$

where γ_i is the command angle for wheel No. $1, 2, \cdots, n$. Since the wheels are placed to be simple, the angle command of robot wheels is considered to be zero (this angle has a value in Swedish and circular wheels). Hence, the value of γ_i would always be zero in Eqs. (3) and (4). $\dot{\rho}_i$ is the longitudinal slip velocity and $\dot{\eta}_i$ is the lateral slip velocity. For this mobile robot, the values of the right-hand side of Eqs. (3) and (4) are constant in view of the characteristics of wheels (not able to be guided). Next, the constraint matrix Λ, which is a $n \times n$ matrix, is obtained by Eqs. (5) and (6) as shown in Box I.

3.1. Calculation of the kinetic energy of the mobile robot with N parallel axles

The kinetic energy (T) of the mobile robot includes the base kinetic energy, particle kinetic energy existing between each wheel and base (T_B), motor driving force (T_r), and wheels kinetic energy (T_w). These are found in what follows:

- The kinetic energy of the mobile base
  The kinetic energy of the mobile platform is obtained as:

$$T_B = \frac{1}{2} m_b \dot{\mathbf{R}}_b^T . \dot{\mathbf{R}}_b + \frac{1}{2} \boldsymbol{\omega}_b^T . \mathbf{I}_b . \boldsymbol{\omega}_b. \tag{7}$$

- The kinetic energy of the particle located between the wheel and base
  Between the base and wheel, there exists a particle that is connected to the base via a parallel spring and damper. Another parallel spring and damper connect the particle to the wheel. Previous studies neglected the impact of spring on the base motion, whereas this study considers the effect of spring on the base and particle along with the effect of

spring on the particle and wheel. The velocity of the ith particle located between two springs and two dampers is written as:

$$\mathbf{V}_i = \dot{h}_i \mathbf{k} + \boldsymbol{\omega}_b \times \mathbf{r}_{i/b}. \quad (8)$$

Moreover, its kinetic energy is obtained as:

$$T_m = \frac{1}{2}\sum_{i=1}^{2n} T_{mi} = \frac{1}{2}\sum_{i=1}^{n} m_{L_i}\{\dot{h}_i^T.\dot{h}_i + 2\dot{h}_i^T.\mathbf{W}_i + \mathbf{W}_i{}^T.\mathbf{W}_i\}, \quad (9)$$

where m_{L_i} is the mass of the particle, and $\mathbf{W}_i = \boldsymbol{\omega}_b \times \mathbf{r}_{i/b}$.

- The kinetic energy of wheels
  By considering the mass and moment of inertia of robot wheels, the associated kinetic energy is obtained as:

$$T_w = \frac{1}{2}\sum_{j=1}^{2n}\left(m_w\left(\dot{\rho}_j^2 + \dot{\eta}_j^2\right) + I_{wy}\dot{\theta}_j^2 + I_{wz}\dot{\varphi}^2\right), \quad (10)$$

  where m_w is the mass of each wheel, I_{wz} is the moment of inertia of each wheel about the z-axis, and I_{wy} is the moment of inertia of each wheel about the y-axis.
- The kinetic energy of the motor
  Each robot wheel is attached to the robot using the connections of motors placed on it. As a result, with the assumption of flexible joints, similar to what was considered in the manipulator for flexible joints, one can obtain accurate models for motors and the connection of mobile robot wheels. Consequently, by calculating the equivalent kinetic energy of each wheel's joint, its effect in the equations is taken into account. In this model, the torque applied to each of these motors is assumed to be in the form of a torsion spring. Then the spring angle changes, and the motion are transferred. The kinetic energy due to the driving forces is in the form presented as:

$$T_r = \frac{1}{2}\sum_{i=1}^{2n} J_r^i \dot{\theta}_{mi}^2, \quad (11)$$

  where J_r^i is the moment of inertia of motors, and $\dot{\theta}_{mi}$ is the angular velocity exerted on the motors of wheels.

3.2. Calculation of the potential energy of the mobile robot with N parallel axles

The potential energy of a robot depends on its configuration or pose. For a robot with N parallel axles, each axle can be raised or lowered independently:

- Kinetic energy stored in springs
  To calculate the potential energy of springs used in the structure of the mobile robot, the position of each spring is first calculated. Next, the displacement of each spring is found using the obtained positions:

$$\mathbf{R}_j = \mathbf{R}_b + \mathbf{L}_j \qquad j = 1, 3, 5, \ldots 2n-1, \quad (12)$$

  where $\mathbf{R}_j$ is the position of the springs' endpoints. The displacement of springs is found to be in the form:

$$\boldsymbol{\delta}_j = L_0\mathbf{k} - \{(\mathbf{R}_b + \mathbf{L}_j).\mathbf{k} - h_j\mathbf{k}\} \qquad j = 1, 3, 5, \ldots 2n-1, \quad (13)$$

  where $\boldsymbol{\delta}_j$ is the displacement of springs along the vertical inertia direction, L_0 is the initial length of springs, $\mathbf{L}_j$ is the vector connecting the initial position of spring to the base center of mass, h_j is the height at which the spring bases are installed, and $\mathbf{k}$ is the unit vector of vertical inertia axis.

$$\mathbf{R}_k = (\mathbf{R}_b + \mathbf{L}_j)\mathbf{k} + \boldsymbol{\delta}_j\mathbf{k} \qquad k = 2, 4, 6, \ldots, 2n, \quad (14)$$

  where $\mathbf{R}_k$ is the position of the springs' endpoints between the particle and wheel. Next, the displacement of lower springs is obtained as:

$$\boldsymbol{\delta}_k = L_0\mathbf{k} - (\mathbf{R}_k\mathbf{k} - h_k\mathbf{k}) \qquad k = 2, 4, 6, \ldots, 2n. \quad (15)$$

  Finally, the total potential energy stored in springs is found as:

$$U_{springs} = \sum_{i=1}^{2n} U_{spring(i)} = \sum_{i=1}^{2n}\frac{1}{2}K_i\boldsymbol{\delta}_i^T.\boldsymbol{\delta}_i, \quad (16)$$

  where K_i represents the stiffness coefficient of springs.
- The potential energy of flexible joints
  Flexible joints bring about potential energy in wheels, as denoted by:

$$U_r = \sum_{i=1}^{2n} U_{ri} = \frac{1}{2}\sum_{i=1}^{2n} K_i^t(\theta_i - \theta_{mi})^2, \quad (17)$$

  where K_i^t is the stiffness coefficient of motors. The total potential energy is written as:

$$U = \sum_{i=1}^{2n} U_{springi} + \sum_{i=1}^{2n} U_{ri}. \quad (18)$$

3.3. Rayleigh dissipation function of a mobile robot with N parallel axes

The dissipated energy in the damper is in the form:

$$U_F = \sum_{i=1}^{2n} U_{F_i} = \sum_{i=1}^{2n} \frac{1}{2} C_i \dot{\boldsymbol{\delta}}^T{}_i . \boldsymbol{\delta}_i, \tag{19}$$

where C_i is the damping coefficient of wheels, and $\dot{\boldsymbol{\delta}}_i$ is their displacement velocity. To calculate the Rayleigh dissipation function, Eq. (15) is differentiated with respect to time and then substituted into Eq. (19). The displacement rate of each damper is found to be as:

$$\dot{\boldsymbol{\delta}}_j = -\{(\dot{\mathbf{R}}_b + \dot{\mathbf{L}}_j)\mathbf{k}.\mathbf{k} - \dot{h}_j \mathbf{k}\} \quad j = 1, 3, 5, ...2n-1. \tag{20}$$

To calculate the displacement rate of springs between particle and wheel, one should take the derivative of their displacements:

$$\dot{\boldsymbol{\delta}}_k = -(\dot{\mathbf{R}}_k^T \mathbf{k} - \dot{h}_k \mathbf{k}) \qquad k = 2, 4, 6, ..., 2n, \tag{21}$$

where $\dot{\mathbf{R}}_k$ is calculated as:

$$\dot{\mathbf{R}}_k = (\dot{\mathbf{R}}_b + \dot{\mathbf{L}}_j)\mathbf{k} + \dot{\boldsymbol{\delta}}_j \mathbf{k}. \tag{22}$$

Next, the Rayleigh dissipation function for the proposed system is found by substituting Eqs. (20) and (21) into Eq. (19).

3.4. Dynamic motion equations of a mobile robot with N parallel axles

To derive the final motion equations of a mobile robot with N parallel axes, one should take the derivatives of Eqs. (18) and (19) as well as system kinetic energy with respect to generalized coordinates and substitute them into Eq. (23). The procedures for obtaining these equations are separately described for potential energy, Rayleigh dissipation function, and base kinetic energy in Appendices A and B. The following explains the classification of the final equation, Eq. (23), and the creation of the system inertia matrix:

$$\frac{d}{dt}\left(\frac{\partial T}{\partial \dot{\boldsymbol{\Theta}}_i}\right) - \frac{\partial T}{\partial \boldsymbol{\Theta}_i} + \frac{\partial U}{\partial \boldsymbol{\Theta}_i} + \frac{\partial U_F}{\partial \dot{\boldsymbol{\Theta}}_i} = \mathbf{Q}_i \qquad i = 1, \ldots, 2n. \tag{23}$$

- Calculation of system inertia matrix
  According to the provided description, by grouping the coefficients of terms in Eq. (23), the matrices of mass, damping, gravity, and Coriolis are formed. These matrices are demonstrated in Appendix C.
- Effect of motion friction between robot and wheel
  Based on previous explanations, friction is a nonlinear phenomenon that is considered in the equations as the loss of applied force and torque. In view of Eq. (23), by taking the effect of friction into account, the final form would be as:

$$\frac{d}{dt}\left(\frac{\partial T}{\partial \dot{\boldsymbol{\Theta}}_i}\right) - \frac{\partial T}{\partial \boldsymbol{\Theta}_i} + \frac{\partial U}{\partial \boldsymbol{\Theta}_i} + \frac{\partial U_F}{\partial \dot{\boldsymbol{\Theta}}_i} + \mathbf{F}\left(\dot{\boldsymbol{\Theta}}\right) = \mathbf{Q}_i. \tag{24}$$

Accordingly, the vector of the wheels friction force, $\mathbf{F}\left(\dot{\boldsymbol{\Theta}}\right)$, can be written as:

$$\mathbf{F}\left(\dot{\boldsymbol{\Theta}}\right) = [0_{1\times 6} \ -f_{lat_1} \ \cdots \ -f_{lat_i} \ -f_{lon_1} \ \cdots \ -f_{lon_i} \ rf_{lon_1} \ \cdots rf_{lon_i} \ 0_{1\times n}]^T \qquad i = 1, 2, ..., n. \tag{25}$$

In which the lateral traction of the ith wheel is f_{lat_i}, and the longitudinal traction counterpart is shown by f_{lon_i} [28].

- Applying kinematic constraints
  The existence of non-holonomic constraints in each axle of the robot under study is required. In view of the kinematic constraints obtained according to the matrix in Eq. (5) and using the method of Lagrange multipliers and Eq. (26), these constraints are applied in the derived motion equation in the form:

$$\boldsymbol{\Lambda}(\boldsymbol{\Theta})\dot{\boldsymbol{\Theta}} = 0. \tag{26}$$

The body motion equations are obtained with the aid of Lagrange multipliers, as in:

$$\mathbf{H}\left(\boldsymbol{\Theta}, \dot{\boldsymbol{\Theta}}\right)\ddot{\boldsymbol{\Theta}} + \mathbf{C}\left(\boldsymbol{\Theta}, \dot{\boldsymbol{\Theta}}\right) + \mathbf{G}(\boldsymbol{\Theta}) + \mathbf{F}\left(\dot{\boldsymbol{\Theta}}\right) + \mathbf{A}(\boldsymbol{\Theta})^T \sigma = \mathbf{Q}. \tag{27}$$

Using $\mathbf{S}(\boldsymbol{\Theta})$ as a null space of the constraint matrix $\boldsymbol{\Lambda}(\boldsymbol{\Theta})$, and then multiplying both sides of Eq. (27) by $\mathbf{S}^T$, the Lagrange multipliers are removed. Finally, one arrives at:

$$\mathbf{S}^T\mathbf{H}\left(\boldsymbol{\Theta}, \dot{\boldsymbol{\Theta}}\right)\ddot{\boldsymbol{\Theta}} + \mathbf{S}^T\mathbf{C}_{1ij}\dot{\boldsymbol{\Theta}} + \mathbf{S}^T\mathbf{C}_{2i} + \mathbf{S}^T\mathbf{G}(\boldsymbol{\Theta}) + \mathbf{S}^T\mathbf{F}\left(\dot{\boldsymbol{\Theta}}\right) = \tau. \tag{28}$$

Substituting the vector values of $\ddot{\boldsymbol{\Theta}}$, and $\dot{\boldsymbol{\Theta}}$ in Eq. (28), the final form is obtained as:

$$\mathbf{S}^T\mathbf{H}\left(\boldsymbol{\Theta}, \dot{\boldsymbol{\Theta}}\right)\left[\dot{\mathbf{S}}(\boldsymbol{\Theta})\dot{\xi} + \mathbf{S}(\boldsymbol{\Theta})\ddot{\xi}\right] + \mathbf{S}^T\mathbf{C}_{1ij}\left[\mathbf{S}(\boldsymbol{\Theta})\dot{\xi}\right] + \mathbf{S}^T\mathbf{C}_{2i} + \mathbf{S}^T\mathbf{G}(\boldsymbol{\Theta}) + \mathbf{S}^T\mathbf{F}\left(\dot{\boldsymbol{\Theta}}\right) = \tau, \tag{29}$$

$$\bar{\mathbf{H}}\ddot{\xi} + \bar{\mathbf{C}}_1\dot{\xi} + \bar{\mathbf{C}}_2 + \bar{\mathbf{G}} + \bar{\mathbf{F}} = \tau, \tag{30}$$

where,

$$\bar{\mathbf{H}} = \mathbf{S}^T\mathbf{H}\left(\boldsymbol{\Theta}, \dot{\boldsymbol{\Theta}}\right)\mathbf{S};$$

$$\bar{\mathbf{C}}_1 = \mathbf{S}^T(\boldsymbol{\Theta})\mathbf{H}\left(\boldsymbol{\Theta}, \dot{\boldsymbol{\Theta}}\right)\dot{\mathbf{S}}(\boldsymbol{\Theta}) + \mathbf{S}^T(\boldsymbol{\Theta})\mathbf{C}_{1ij}\left(\boldsymbol{\Theta}, \dot{\boldsymbol{\Theta}}\right)\mathbf{S}(\boldsymbol{\Theta});$$

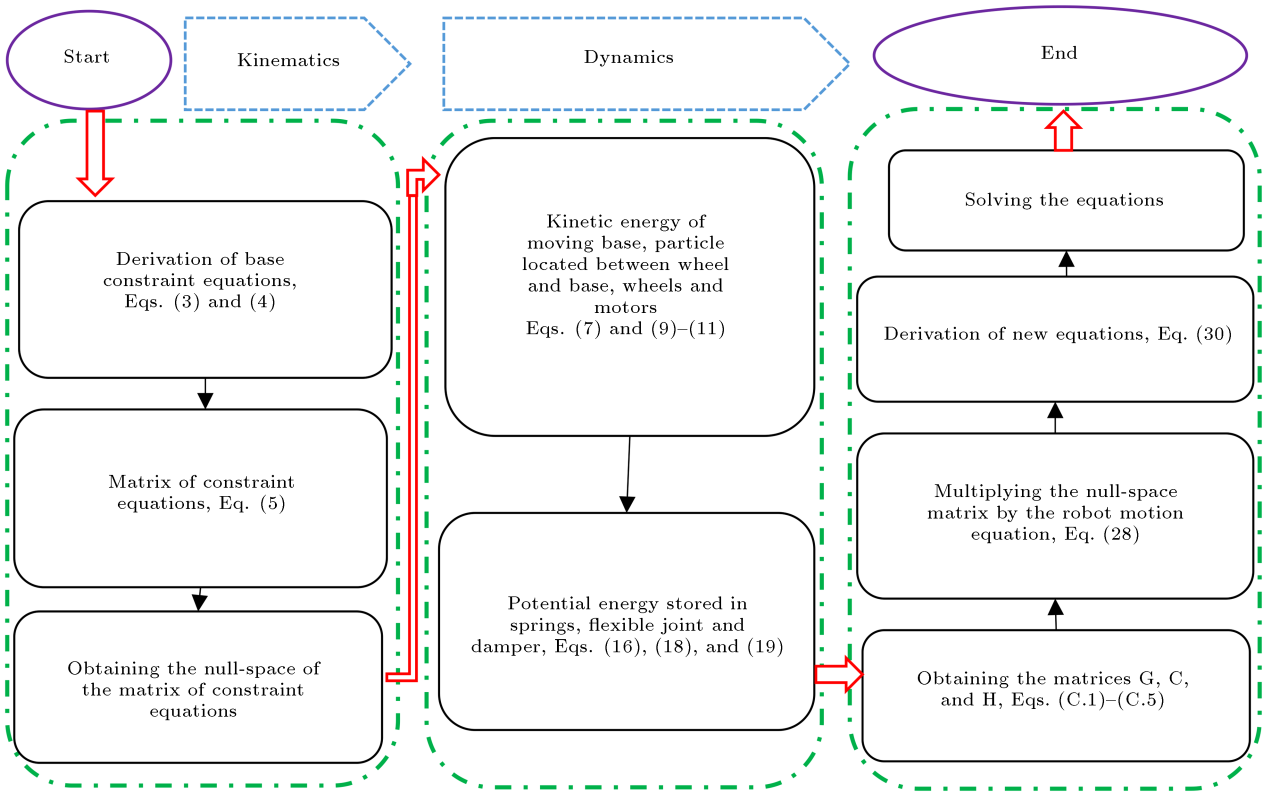

Figure 3. Motion equations derivation flowchart.

$$\bar{\mathbf{C}}_2 = \mathbf{S}^T \mathbf{C}_{2i};$$

$$\bar{\mathbf{F}} = \mathbf{S}^T(\boldsymbol{\Theta})\,\mathbf{F}\left(\dot{\boldsymbol{\Theta}}\right);$$

$$\bar{\mathbf{G}} = \mathbf{S}^T(\boldsymbol{\Theta})\,\mathbf{G}(\boldsymbol{\Theta});$$

$$\tau = \mathbf{S}^T(\boldsymbol{\Theta})\,\mathbf{Q}. \tag{31}$$

Figure 3 represents the Euler-Lagrange formulation flowcharts imported to evaluate the motion equations of the defined system.

4. Simulation and analysis of numerical results

The software simulation or experimental component will be the main approach for evaluating the concluded system performance and preparing the report about model accuracy. Consequently, in this paper, the system's performance was examined, and the efficiency of the dynamic model was compared based on various environmental conditions along with the system's characteristics. Accordingly, the results of both numerical and analytical analyses are discussed. To validate the accuracy of the obtained mathematical model, software simulation is carried out using MATLAB for a four-wheeled mobile robot while longitudinal and lateral wheel's slip, backlash, and flexibility of each of its wheel's motor are considered. The studied robot, similar to what is shown in Figure 4, benefits from one electric motor in each of its wheels. In addition, the suspension system is employed on each wheel, composed of two successive spring-damper systems. The robot's motion starts from the stationary state according to the applied torque to the wheels. To compare the results and check the derived equations, the motion is investigated on different surfaces. In addition, the different longitudinal and lateral traction forces, along with the various damping and stiffness coefficients for the suspension system, were studied. As a result, based on Eq. (6), the generalized coordinates of the system are:

$$\boldsymbol{\Theta} = [\mathbf{R}_b^T \boldsymbol{\Omega}_b^T \eta_1 \dots \eta_4 \rho_1 \dots \rho_4 \quad \theta_1 \dots \theta_4 \theta_{m1} \dots \theta_{m4}]^T. \tag{32}$$

The robot parameters used in the simulation process are listed in Table 1. This robot has 22 degrees of freedom in four-wheeled mode. And for each wheel, 4 degrees of freedom are added to transactions. Therefore, the equations require 38 degrees of freedom to solve for an 8-wheeled robot. As a result, the time to solve the equations is very long. Also, Eq. (30) is updated as follows:

$$\bar{\mathbf{H}}_{22\times 22}\ddot{\boldsymbol{\xi}}_{22\times 1} + \bar{\mathbf{C}}_{1_{22\times 22}}\dot{\boldsymbol{\xi}}_{22\times 1} + \bar{\mathbf{C}}_{2_{22\times 1}} + \bar{\mathbf{G}}_{22\times 1} + \bar{\mathbf{F}}_{22\times 1} = \boldsymbol{\tau}_{22\times 1}. \tag{33}$$

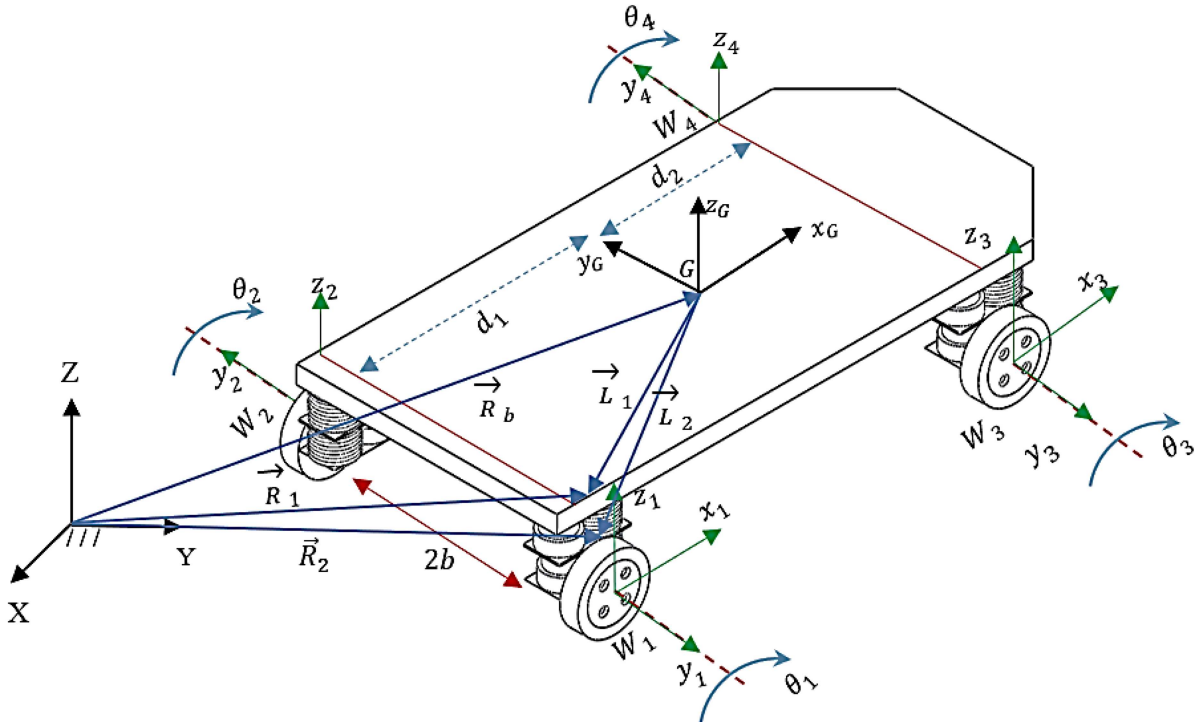

Figure 4. Four-wheeled mobile robot.

Table 1. Required parameters for simulation of four-wheeled mobile robot.

Parameter	Value	Unit
Motor stiffness coefficient	$K_1^t = K_2^t = K_3^t = K_4^t = 1000$	N.M
Motor moment of inertia/	$J_{r1} = J_{r2} = J_{r3} = J_{r4} = 1 \times 10^{-4}$	kg.m
Base mass	$m_b = 10$	kg
Wheel mass	$m_w = 0.5$	kg
Base moment of inertia about z	$I_{bz} = 0.3701$	kg.m^2
Base moment of inertia about x	$I_{bx} = 0.0708$	kg.m^2
Base moment of inertia about y	$I_{by} = 0.3007$	kg.m^2
Wheel moment of inertia about y	$I_{wy} = 0.0004$	kg.m^2
Wheel moment of inertia about z	$I_{wz} = 0.0002$	kg.m^2
Distance between axle and base center of mass	$d_1 = d_2 = 0.24$	m
Half-width of base	$b = 0.145$	m
Wheel radius	$r = 0.04$	m
Initial spring length	$L_{01}, ..., L_{08} = 0.03$	m
Particle mass	$m_{L1} = m_{L2} = m_{L3} = m_{L4} = 0.04$	kg
Wheels torque	if $t \geq 0$ & $t < 1$ $\tau_1 = \tau_3 = 1$; $\tau_2 = \tau_4 = 1$ if $t \geq 1$ & $t < 2$ $\tau_1 = \tau_3 = 0$; $\tau_2 = \tau_4 = 2$ elseif $t \geq 2$ & $t < 4$ $\tau_1 = \tau_3 = 0$; $\tau_2 = \tau_4 = 0$	N.M

According to the presented description about implementing the simulation on different surfaces, the data on the longitudinal and lateral traction forces on two different surfaces of ice and loose gravel, which is used in Eq. (33), are provided in Table 2. To investigate the effect of damping and spring stiffness variations employed in the robot suspension system on loose gravel and ice, these coefficients' variations have been considered in the simulation process.

Figure 5 shows the rotations of wheels No. 1 and 2 as an example: each wheel is simulated on two surface cases, and the rotations of each wheel and its motor are separately presented. According to the concluded results, the rotations of wheels No. 1 and 2 are not

Table 2. Four different surfaces for the robot motion [28].

Surface	Longitudinal and lateral traction forces	Stiffness and damping coefficient
(1) Loose gravel	$\begin{cases} F_{lon} = 56 \text{ N} & Sr = 0 - 0.4 \\ F_{lat} = 4 \text{ N} & Sa = 0 - 10 \text{ (deg)} \ \& \ \mu = 0.06 \end{cases}$	$\begin{cases} C_{1\ldots4} = 55 \text{ Ns/m} & C_{5\ldots8} = 60 \text{ Ns/m} \\ K_{1\ldots4} = 180 \text{ N/m} & K_{5\ldots8} = 185 \text{ Ns/m} \end{cases}$
(2) Ice	$\begin{cases} F_{lon} = 4.25 \text{ N} & Sr = 0 - 0.4 \\ F_{lat} = 4 \text{ N} & Sa = 0 - 10 \text{ (deg)} \ \& \ \mu = 0.06 \end{cases}$	$\begin{cases} C_{1\ldots4} = 55 \text{ Ns/m} & C_{5\ldots8} = 60 \text{ Ns/m} \\ K_{1\ldots4} = 180 \text{ N/M} & K_{5\ldots8} = 185 \text{ Ns/m} \end{cases}$
(3) Loose gravel	$\begin{cases} F_{lon} = 56 \text{ N} & Sr = 0 - 0.4 \\ F_{lat} = 4 \text{ N} & Sa = 0 - 10 \text{ (deg)} \ \& \ \mu = 0.06 \end{cases}$	$\begin{cases} C_{1\ldots4} = 50 \text{ Ns/m} & C_{5\ldots8} = 55 \text{ Ns/m} \\ K_{1\ldots4} = 180 \text{ N/m} & K_{5\ldots8} = 185 \text{ N/m} \end{cases}$
(4) Loose gravel	$\begin{cases} F_{lon} = 56 \text{ N} & Sr = 0 - 0.4 \\ F_{lat} = 4 \text{ N} & Sa = 0 - 10 \text{ (deg)} \ \& \ \mu = 0.06 \end{cases}$	$\begin{cases} C_{1\ldots4} = 0 & C_{5\ldots8} = 0 \\ K_{1\ldots4} = 0 & K_{5\ldots8} = 0 \end{cases}$

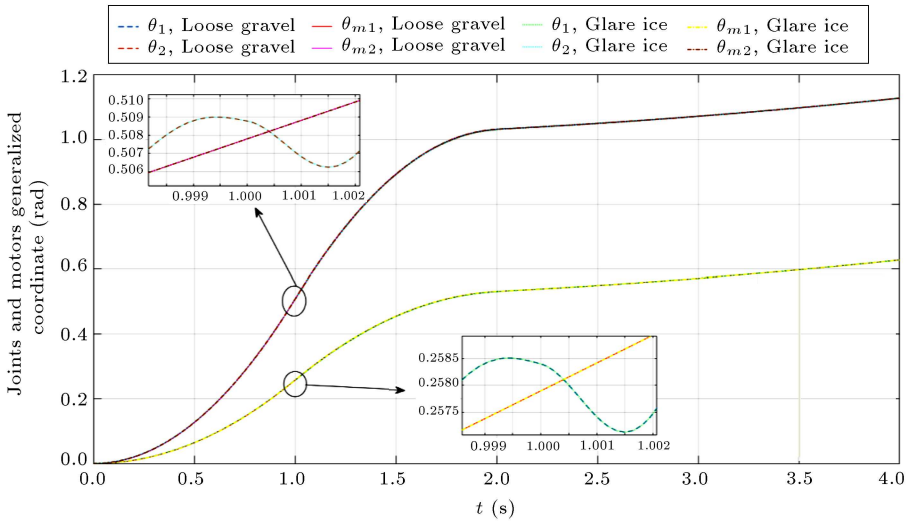

Figure 5. Rotation of wheel and motor.

identical, while the imported torques to both of them are the same. Therefore, it can be concluded that the wheels' slip cause longitudinal and lateral moving, which are undesirable.

On the other hand, these differences between the rotations of the wheels lead to the robot rotating on the floor. It means that the robot deviates from the desired path. Additionally, the amount of rotation of the robot motor and wheels is such that the change in the angle of wheels during motion oscillates with the change in the motor angle. The oscillation domain depends on the motor's flexibility. This means that the robot wheels experience slip, and motor rotation is not completely transferred to the robot wheel with similar velocity. Figure 6 shows that the angular velocity of wheels and robot motors is similar to what was previously explained. The angular velocity of wheel No. 2 is almost twice that of wheel No. 1. Moreover, the plot of the angular velocity of oscillating wheels is drawn about the plot of the angular velocity of motors. In view of the exerted torque to the motors, as the direction of torque changes at $t = 1$ s, the amplitude of oscillations increases. Finally, after 2 seconds from the onset of motion, although no torque is exerted on the motors, the wheels' oscillation continues. It should be mentioned that the effect of changing the surface coefficients, in view of the definition of longitudinal and lateral slip variables, does not affect the change of angle and angular velocity of wheels and motors.

Figure 7 represents the mobile robot's motion in space. As expected, the robot deviates to a lesser extent on ice, while the resulting deviation on loose gravel under similar conditions is around twice as much. As expected, the longitudinal motion on ice is more on ice than on loose gravel. These indicate that the amount of rolling is more on loose gravel, preventing the longitudinal motion of the robot and allowing the lateral motion instead. Figure 8 displays the rotation of robot wheels in two different cases. The effect of the spring and dampers of each wheel's suspension system

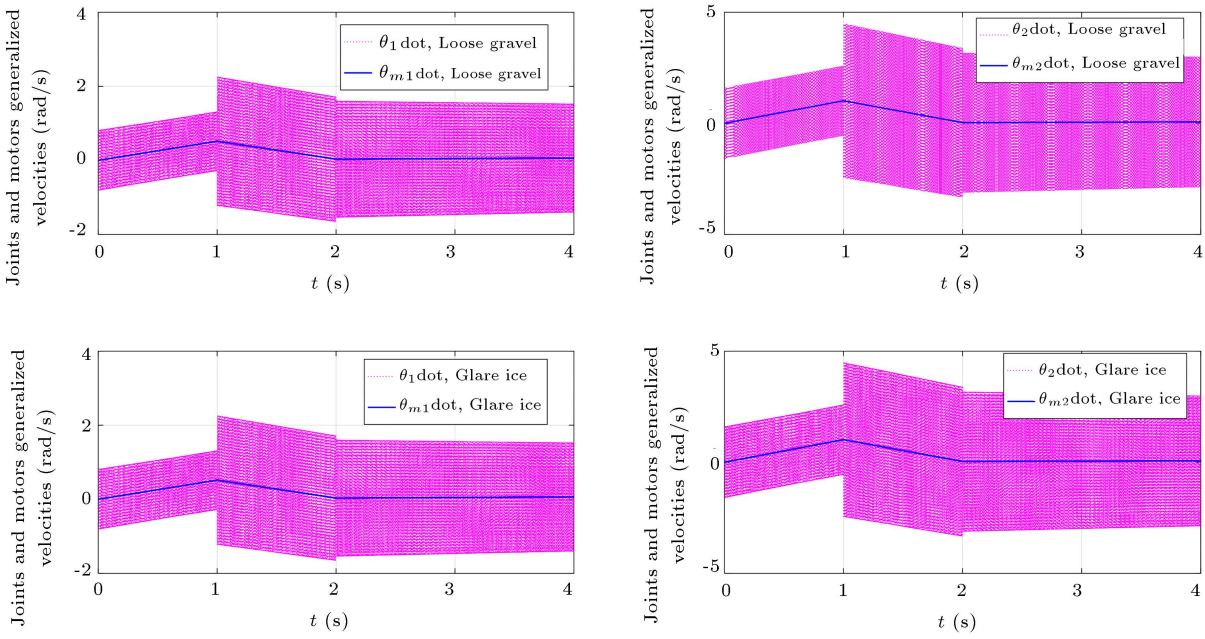

Figure 6. Angular velocity of wheel and motor.

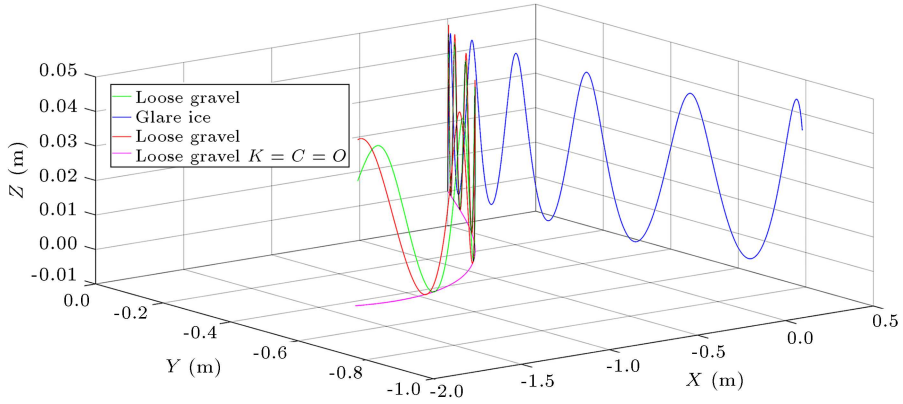

Figure 7. Motion on the plane x, y, and z.

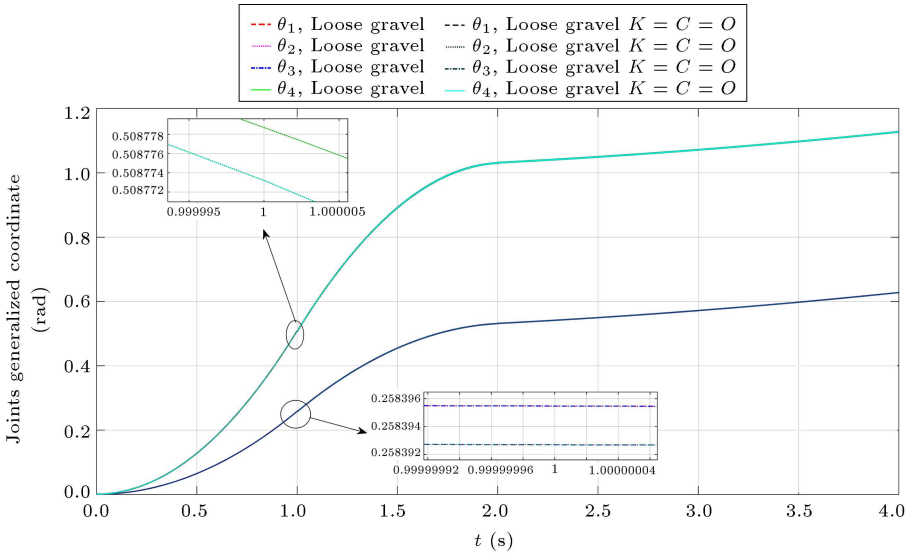

Figure 8. Rotations of wheels No. 1 to 4.

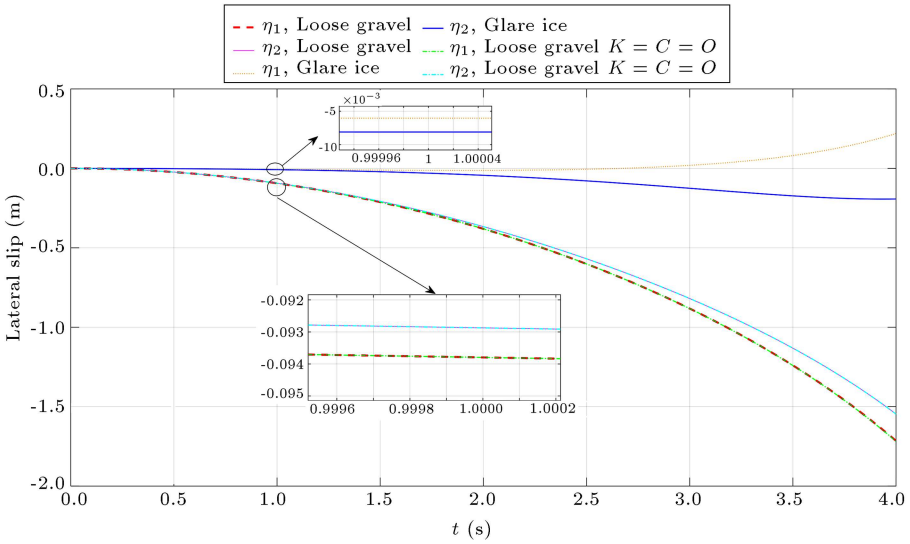

Figure 9. Lateral slip.

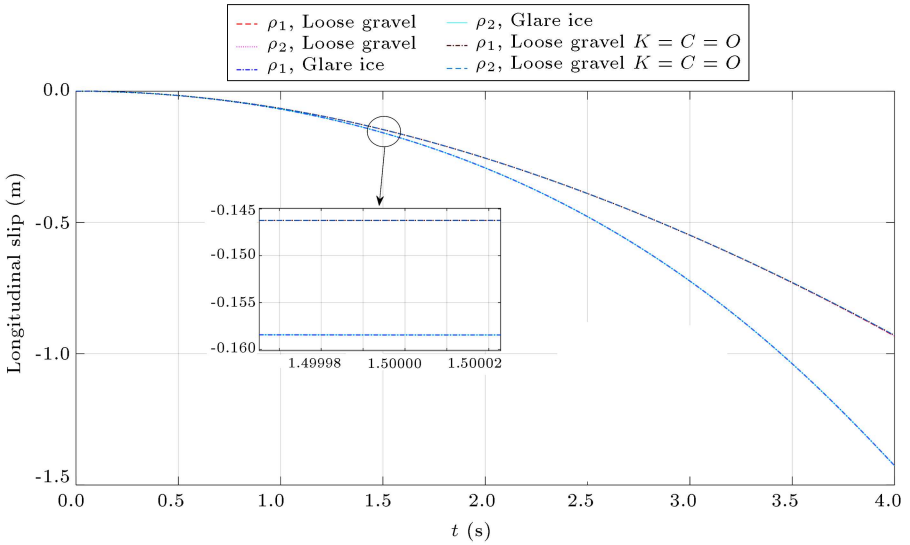

Figure 10. Longitudinal slip.

can be observed in one case, while this is disregarded in the other. On the other hand, the presented results suggest that the motions of wheels No. 1 and 3, as well as wheels No. 2 and 4, are similar, with only minor differences.

Figures 9 and 10 show the longitudinal and lateral slips of the robot, respectively. As is shown in the figures and besides, these results are pointed out in Figure 7. According to Figure 9, the sideways motion of the robot on various surfaces differs based on each wheel. The variables related to wheels No. 1 and 2 are displayed. The lateral slip of wheels No. 1 and 2 on the ice takes place along negative and positive directions, indicating the slippage of the wheels. Regarding the slip of wheels No. 1 and 2 on loose gravel, one can notice that slip occurs in one direction, with different slippage values for each wheel. The effect of the spring and damper of the suspension system of the robot on this parameter brings about a difference. Concerning longitudinal slip, the results do not demonstrate the expressed difference of lateral slip.

Figure 11 shows the longitudinal slip velocity and robot wheels as an example. The influence of the surface, according to the mentioned explanations, is subtle during longitudinal motion, whereas the coefficients of the damper and spring in the suspension system are consequential. Figure 12 shows the effect of the coefficients of the damper and spring on the motion along the z-direction of the robot.

5. Conclusion

In this study, the dynamic equations of an extended mobile robot with parallel axles are studied. Each axis

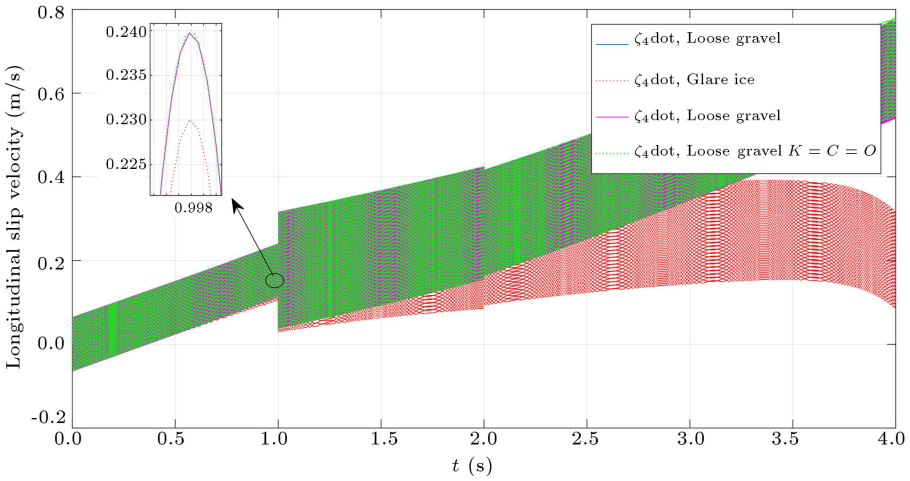

Figure 11. Longitudinal slip velocity.

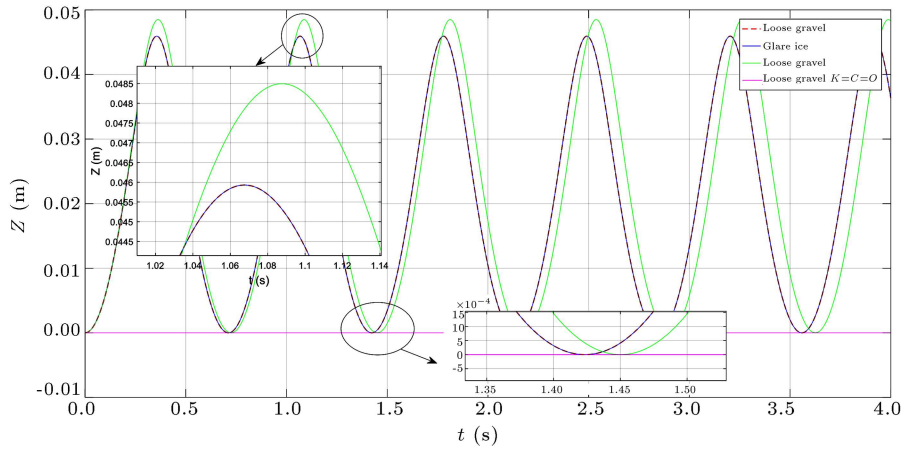

Figure 12. Motion the robot in line z.

has two wheels with independent functions. The Euler-Lagrange formulation is utilized to obtain the motion equations of the robotic system. The main difference between the determined model with the previous ones is not only limited to the new platform design but also, in view of the necessity of accurate motion and applicability on uneven surfaces for multiple-axle mobile robots, the equations are derived by considering the effect of longitudinal and lateral slip for all wheels. In addition, the suspension system is intended with two springs and two dampers. By reviewing the motors joint flexibility consideration's effect on manipulator dynamic performances, it concluded that motion accuracy and control of the robot depend on the motor performance on every wheel as well. Accordingly, each wheel's motors model should be considered as it was modeled in a manipulator's flexible joint. Noting the concluded motion equations and the existence of non-holonomic constraints in the robot platform, the final equations are developed using the Lagrange multiplier approach. After examining the results from simulating the motion equations for a mobile robot with four wheels, it becomes clear that the robot performs differently on ice and also loose gravel, remembering that the simplified model is not applicable in this case. Moreover, it is observed that with the passage of time, the amount of longitudinal and lateral slip of the robot increases compared with the initial case. The exact location of the robot at all instances of time is found by calculating these quantities. By comparing the results, the effect of the traction surface caused by loose gravel and ice on the motion type of robot becomes evident. One can be observed that the longitudinal motion of the robot is less on a surface composed of loose gravel, and lateral slip occurs due to the involvement of the wheel in loose gravel. The amount of longitudinal slip is more on the ice, while the lateral slip decreases. The obtained mathematical model can be employed in designing rescue and exploration robots with different dimensions and various mobile axles.

Nomenclature

C_i	Damping coefficient of wheels

C	Inertia matrix
$\boldsymbol{F}\left(\dot{\boldsymbol{\Theta}}\right)$	Vector of wheels friction force
$\boldsymbol{G}$	Robot center of mass
$\mathbf{H}_{ij}$	Matrices of mass
I_{bz}	Base moment of inertia about z
I_{by}	Base moment of inertia about y
I_{bx}	Base moment of inertia about x
I_{wz}	Wheel moment of inertia about z
I_{wy}	Wheel moment of inertia about y
$\mathbf{I}_b$	Base moment of inertia
J_r^i	Moment of inertia of motors
K_i	Represents the stiffness coefficient of springs
K_i^t	Stiffness coefficient of motors
L_0	Initial spring length
$\boldsymbol{L}_j$	Vector connecting the initial position of spring to the base center of mass
$\mathbf{R}_j$	Position of springs' endpoints
$\mathbf{R}_b^T$	Position of robot center of mass (point $\mathbf{G}$)
$\mathbf{S}(\boldsymbol{\Theta})$	Null-space of the constraint matrix $\boldsymbol{\Lambda}(\boldsymbol{\Theta})$
T	Kinetic energy
T_B	Particle kinetic energy existing between each wheel and base
T_r	Motor driving force kinetic energy
T_w	Wheels kinetic energy
$U_{springs}$	Total potential energy stored in springs
U_{ri}	Potential energy of flexible joints
U_F	Dissipated energy in the damper
b	Half-width of base
d_i	Distance between axle and base center of mass
f_{lon_i}	Longitudinal traction of ith wheel
f_{lat_i}	Lateral traction of ith wheel
m_{L_i}	Mass of the particle between two springs and two dampers
m_w	Mass of each wheel
m_b	Base mass
h_j	Height at which the spring bases are installed
G	Gravity acceleration
γ_i	Command angle
$\boldsymbol{\delta}_j$	Displacement of springs along the vertical inertia direction
η	Lateral slip
θ	Exerted angles wheels
θ_m	Exerted angles motors
θ_r	Yaw
θ_p	Pitch
$\boldsymbol{k}$	Unit vector of vertical inertia axis
ρ	Longitudinal slip
φ	Roll
$\boldsymbol{\omega}_b$	Angular velocity of base
$\boldsymbol{\theta}$	Vectors of generalized coordinates
Λ	Constraint matrix
$\boldsymbol{\Omega}_b^T$	Euler angles

References

1. Comellas, M., Pijuan, J., Nogués, M., et al. "Influence of the transmission configuration of a multiple axle vehicle on the obstacle surmounting capacity", *Vehicle System Dynamics*, **52**(9), pp. 1191–1210 (2014).
2. Trojnacki, M. "Modeling and motion simulation of a three-wheeled mobile robot with front wheel driven and steered taking into account wheels' slip", *Archive of Applied Mechanics*, **83**(1), pp. 109–124 (2013).
3. Taghia, J., Wang, X., Lam, S., et al. "A sliding mode controller with a nonlinear disturbance observer for a farm vehicle operating in the presence of wheel slip", *Autonomous Robots*, **41**(1), pp. 71–88 (2017).
4. Smieszek, M., Dobrzanska, M., and Dobrzanski, P. "The impact of load on the wheel rolling radius and slip in a small mobile platform", *Autonomous Robots*, **43**(8), pp. 2095–2109 (2019).
5. Dogru, S. and Marques, L. "Power characterization of a skid-steered mobile field robot with an application to headland turn optimization", *Journal of Intelligent and Robotic Systems*, **93**(3–4), pp. 601–615 (2019).
6. Korayem, M.H. and Nekoo, S.R. "The SDRE control of mobile base cooperative manipulators: Collision free path planning and moving obstacle avoidance", *Robotics and Autonomous Systems*, **86**, pp. 86–105 (2016).
7. Zhao, Z., Liu, H., Chen, H., et al. "Kinematics-aware model predictive control for autonomous high-speed tracked vehicles under the off-road conditions", *Mechanical Systems and Signal Processing*, **123**, pp. 333–350 (2019).
8. Reina, G. and Galati, R. "Slip-based terrain estimation with a skid-steer vehicle", *Vehicle System Dynamics*, **54**(10), pp. 1384–1404 (2016).
9. Korayem, M.H., Dehkordi, S.F., and Mehrjooee, O. "ScienceDirect nonlinear analysis of open-chain flexible manipulator with time-dependent structure", *Advances in Space Research*, **69**(2), pp. 1027–1049 (2022).
10. Wiech, J., Eremeyev, V.A., and Giorgio, I. "Virtual spring damper method for nonholonomic robotic swarm self-organization and leader following", *Continuum Mechanics and Thermodynamics*, **30**(5), pp. 1091–1102 (2018).

11. Ahmad Abu Hatab, R.D. "Dynamic modelling of differential-drive mobile robots using lagrange and newton-euler methodologies: A unified framework", *Advances in Robotics and Automation*, **2**(2), pp. 1–7 (2013).
12. Eslamy, M. and Moosavian, S.A.A. "Control of suspended wheeled mobile robots with multiple arms during object manipulation tasks", *International Conference on Robotics and Automation*, pp. 3730–3735 (2009).
13. Korayem, M.H. and Dehkordi, S.F. "Derivation of motion equation for mobile manipulator with viscoelastic links and revolute-prismatic flexible joints via recursive Gibbs-Appell formulations", *Robotics and Autonomous Systems*, **103**, pp. 175–198 (2018).
14. Alipour, K. and Moosavian, S.A.A. "Effect of terrain traction, suspension stiffness and grasp posture on the tip-over stability of wheeled robots with multiple arms", *Advanced Robotics*, **26**(8–9), pp. 817–842 (2012).
15. Trojnacki, M. and Dąbek, P. "Studies of dynamics of a lightweight wheeled mobile robot during longitudinal motion on soft ground", *Mechanics Research Communications*, **82**, pp. 36–42 (2017).
16. Khan, H., Iqbal, J., Baizid, K., et al. "Longitudinal and lateral slip control of autonomous wheeled mobile robot for trajectory tracking", *Frontiers of Information Technology and Electronic Engineering*, **16**, pp. 166–172 (2015).
17. Trojnacki, M. "Dynamics model of a four-wheeled mobile robot for control applications-A three-case study", *Intelligent Systems*, **323**(8), pp. 100–116 (2015).
18. Chen, M. "Disturbance attenuation tracking control for wheeled mobile robots with skidding and slipping", *Transactions on Industrial Electronics*, **64**(4), pp. 3359–3368 (2017).
19. Jaskot, A. and Spiewak, S. "Motion modeling of the four-wheeled mobile platform under slippage conditions", *Machine Dynamics Research*, **40**(2), pp. 43–53 (2016).
20. Seegmiller, N., Rogers-Marcovitz, F., Miller, G., et al. "A unified perturbative dynamics approach to online vehicle model identification", *Springer Tracts in Advanced Robotics*, **100**(8), pp. 585–601 (2017).
21. Ni, J. and Hu, J. "Handling performance control for hybrid 8-wheel-drive vehicle and simulation verification", *Vehicle System Dynamics*, **54**(8), pp. 1098–1119 (2016).
22. Anwar, Ali, Z., Wang, D., Safwan, M., et al. "Trajectory tracking of a nonholonomic wheeleed mobile robot using hybrid controller", *International Journal of Modeling and Optimization*, **6**(3), pp. 136–141 (2016).
23. Ibrahim, A.E.S.B. "Wheeled mobile robot trajectory tracking using sliding mode control", *Journal of Computer Science*, **12**(1), pp. 48–55 (2016).
24. Song, T., Xi, F. (Jeff), Guo, S., et al. "Slip analysis for a wheeled mobile manipulator", *Journal of Dynamic Systems, Measurement, and Control*, **140**(2), pp. 021005–021017 (2018).
25. Salgado, I., Cruz-Ortiz, D., Camacho, O., et al. "Output feedback control of a skid-steered mobile robot based on the super-twisting algorithm", *Control Engineering Practice*, **58**(10), pp. 193–203 (2017).
26. Habibnejad Korayem, M., Ghobadi, N., and Fathollahi Dehkordi, S. "Designing an optimal control strategy for a mobile manipulator and its application by considering the effect of uncertainties and wheel slipping", *Optimal Control Applications and Methods*, **42**(5), pp. 1487–1511 (2021).
27. Jaskot, A. and Posiadała, B. "Analysis of motion of the three wheeled mobile platform", *MATEC Web of Conferences*, **157**(3), pp. 1–9 (2018).
28. Sidek, S.N. "Dynamic modeling and control of nonholonomic wheeled mobile robot subjected to wheel slip", *Diss. Vanderbilt University*, pp. 66–74 (2008).

Appendix A

Calculation of $\frac{\partial U_F}{\partial \dot{\Theta}_i}$. The steps for differentiation and putting the potential energy rayleigh dissipation function of the mobile robot with n parallel axles in matrix form, as expressed in Eq. (19), are presented:

$$\frac{\partial U_F}{\partial \dot{\boldsymbol{\Theta}}_i} = \frac{1}{2} C_i \left\{ \frac{\partial}{\partial \dot{\boldsymbol{\Theta}}_i} \left(\dot{\boldsymbol{\delta}}^T{}_1 . \dot{\boldsymbol{\delta}}_1 \right) + \frac{\partial}{\partial \dot{\boldsymbol{\Theta}}_i} \left(\dot{\boldsymbol{\delta}}^T{}_2 . \dot{\boldsymbol{\delta}}_2 \right) + \cdots \right\}, \quad \text{(A.1)}$$

and:

$$\frac{\partial}{\partial \dot{\boldsymbol{\Theta}}_i} \left(\dot{\boldsymbol{\delta}}^T{}_1 . \dot{\boldsymbol{\delta}}_1 \right) = \frac{\partial}{\partial \dot{\boldsymbol{\Theta}}_i} \left\{ \left(\sum_{k=1}^{N} \frac{\partial \boldsymbol{\delta}_1}{\partial \boldsymbol{\Theta}_k} \dot{\boldsymbol{\Theta}}_k \right)^T \sum_{s=1}^{N} \frac{\partial \boldsymbol{\delta}_1}{\partial \boldsymbol{\Theta}_s} \dot{\boldsymbol{\Theta}}_s \right\}. \quad \text{(A.2)}$$

Finally, a relation can be written in the form:

$$\left(\sum_{k=1}^{N} \frac{\partial \boldsymbol{\delta}_1}{\partial \boldsymbol{\Theta}_k} \dot{\boldsymbol{\Theta}}_k \right)^T \sum_{s=1}^{N} \frac{\partial \boldsymbol{\delta}_1}{\partial \boldsymbol{\Theta}_s} \dot{\boldsymbol{\Theta}}_s = \sum_{k=1}^{N} \sum_{s=1}^{N} \left(\frac{\partial \boldsymbol{\delta}_1{}^T}{\partial \boldsymbol{\Theta}_k} . \frac{\partial \boldsymbol{\delta}_1}{\partial \boldsymbol{\Theta}_s} \right) \dot{\boldsymbol{\Theta}}_k \dot{\boldsymbol{\Theta}}_s. \quad \text{(A.3)}$$

In view of Eq. (A.3), Eq. (A.1) may be considered as:

$$\left(\frac{\partial U_F}{\partial \dot{\boldsymbol{\Theta}}_i} \right)_1 = \frac{1}{2} C_1 \left\{ \sum_{k=1}^{N} \sum_{s=1}^{N} \left(\frac{\partial \boldsymbol{\delta}_1^T}{\partial \boldsymbol{\Theta}_k} . \frac{\partial \boldsymbol{\delta}_1}{\partial \boldsymbol{\Theta}_s} \right) \dot{\boldsymbol{\Theta}}_k \dot{\boldsymbol{\Theta}}_s \right\}$$

$$= \frac{1}{2}C_1\left[2\frac{\partial \boldsymbol{\delta}_1^T}{\partial \boldsymbol{\Theta}_i}.\frac{\partial \boldsymbol{\delta}_1}{\partial \boldsymbol{\Theta}_1}\cdots\cdots 2\frac{\partial \boldsymbol{\delta}_1^T}{\partial \boldsymbol{\Theta}_i}.\frac{\partial \tilde{\delta}_1}{\partial \boldsymbol{\Theta}_n}\right]$$

$$\begin{bmatrix}\dot{\boldsymbol{\Theta}}_1\\ \vdots\\ \dot{\boldsymbol{\Theta}}_n\end{bmatrix}. \tag{A.4}$$

By simplifying, one arrives at:

$$\left(\frac{\partial U_F}{\partial \dot{\boldsymbol{\Theta}}_i}\right)_1 = C_1\left[\frac{\partial \boldsymbol{\delta}_1^T}{\partial \boldsymbol{\Theta}_i}.\frac{\partial \boldsymbol{\delta}_1}{\partial \boldsymbol{\Theta}_1}\cdots\cdots\frac{\partial \boldsymbol{\delta}_1^T}{\partial \boldsymbol{\Theta}_i}.\frac{\partial \boldsymbol{\delta}_1}{\partial \boldsymbol{\Theta}_n}\right]$$

$$\begin{bmatrix}\dot{\boldsymbol{\Theta}}_1\\ \vdots\\ \dot{\boldsymbol{\Theta}}_n\end{bmatrix}. \tag{A.5}$$

Eq. (A.5) is only applicable to damper No. 1. In general; the following relation can be used:

$$\frac{\partial U_F}{\partial \dot{\boldsymbol{\Theta}}_i} = \left[C_1\frac{\partial \boldsymbol{\delta}_1^T}{\partial \boldsymbol{\Theta}_i}.\frac{\partial \boldsymbol{\delta}_1}{\partial \boldsymbol{\Theta}_1} + C_2\frac{\partial \boldsymbol{\delta}_2^T}{\partial \boldsymbol{\Theta}_i}.\frac{\partial \boldsymbol{\delta}_2}{\partial \boldsymbol{\Theta}_1} + \cdots + C_1\right.$$

$$\left.\frac{\partial \boldsymbol{\delta}_1^T}{\partial \boldsymbol{\Theta}_i}.\frac{\partial \boldsymbol{\delta}_1}{\partial \boldsymbol{\Theta}_N} + C_2\frac{\partial \boldsymbol{\delta}_2^T}{\partial \boldsymbol{\Theta}_i}.\frac{\partial \boldsymbol{\delta}_2}{\partial \boldsymbol{\Theta}_N} + \cdots\right]\boldsymbol{\Theta}. \tag{A.6}$$

Appendix B

Calculation of $\frac{d}{dt}\left(\frac{\partial T_b}{\partial \dot{\boldsymbol{\Theta}}_i}\right) - \frac{\partial T_b}{\partial \boldsymbol{\Theta}_i}$**.** In this appendix, the base kinetic energy is found. To this end, the kinetic energy is divided into two parts, and corresponding values are individually calculated:

$$T_b = \frac{1}{2}m_b\dot{\mathbf{R}}_b^T\dot{\mathbf{R}}_b\frac{\partial T_b}{\partial \dot{\boldsymbol{\Theta}}_i} = \frac{1}{2}m_b$$

$$\left(\frac{\partial \dot{\mathbf{R}}_b^T}{\partial \dot{\boldsymbol{\Theta}}_i}\dot{\mathbf{R}}_b + \dot{\mathbf{R}}_b^T\frac{\partial \dot{\mathbf{R}}_b}{\partial \dot{\boldsymbol{\Theta}}_i}\right) = m_b\left(\frac{\partial \dot{\mathbf{R}}_b^T}{\partial \dot{\boldsymbol{\Theta}}_i}\dot{\mathbf{R}}_b\right). \tag{B.1}$$

Furthermore, it is known that:

$$\frac{\partial \dot{\mathbf{R}}_b^T}{\partial \dot{\boldsymbol{\Theta}}_i} = \frac{\partial \mathbf{R}_b^T}{\partial \boldsymbol{\Theta}_i}. \tag{B.2}$$

Using Eq. (B.2), the Lagrange equation can be presented as:

$$\frac{d}{dt}\left(\frac{\partial T_b}{\partial \dot{\boldsymbol{\Theta}}_i}\right) - \frac{\partial T_b}{\partial \boldsymbol{\Theta}_i}$$

$$= m_b\left(\frac{\partial \dot{\mathbf{R}}_b^T}{\partial \boldsymbol{\Theta}_i}\dot{\mathbf{R}}_b + \frac{\partial \mathbf{R}_b^T}{\partial \boldsymbol{\Theta}_i}\ddot{\mathbf{R}}_b\right)$$

$$- m_b\left(\frac{\partial \dot{\mathbf{R}}_b^T}{\partial \boldsymbol{\Theta}_i}\dot{\mathbf{R}}_b\right) = m_b\left(\frac{\partial \mathbf{R}_b^T}{\partial \boldsymbol{\Theta}_i}\ddot{\mathbf{R}}_b\right). \tag{B.3}$$

By taking the derivative of Eq. (B.2), Eq. (B.3) may be written as:

$$\frac{d}{dt}\left(\frac{\partial T_b}{\partial \dot{\boldsymbol{\Theta}}_i}\right) - \frac{\partial T_b}{\partial \boldsymbol{\Theta}_i}$$

$$= m_b\frac{\partial \mathbf{R}_b^T}{\partial \boldsymbol{\Theta}_i}.\sum_{s=1}^{N}\left\{\frac{\partial}{\partial \boldsymbol{\Theta}_s}\left(\sum_{t=1}^{N}\frac{\partial \mathbf{R}_b}{\partial \boldsymbol{\Theta}_t}\dot{\boldsymbol{\Theta}}_t\right)\dot{\boldsymbol{\Theta}}_s\right\}$$

$$+ m_b\frac{\partial \mathbf{R}_b}{\partial \boldsymbol{\Theta}_i}.\sum_{s=1}^{N}\left\{\frac{\partial \mathbf{R}_b}{\partial \boldsymbol{\Theta}_s}\ddot{\boldsymbol{\Theta}}_s\right\}. \tag{B.4}$$

Finally, by separating the constituents of Eq. (B.4) and converting them into matrix form, one can write:

$$\frac{d}{dt}\left(\frac{\partial T_b}{\partial \dot{\boldsymbol{\Theta}}_i}\right) - \frac{\partial T_b}{\partial \boldsymbol{\Theta}_i}$$

$$= m_b\left[\frac{\partial \mathbf{R}_b^T}{\partial \boldsymbol{\Theta}_i}.\frac{\partial \mathbf{R}_b}{\partial \boldsymbol{\Theta}_1}\cdots\frac{\partial \mathbf{R}_b^T}{\partial \boldsymbol{\Theta}_i}.\frac{\partial \mathbf{R}_b}{\partial \boldsymbol{\Theta}_n}\right]\ddot{\boldsymbol{\Theta}}$$

$$+ m_b\left[\frac{\partial \mathbf{R}_b^T}{\partial \boldsymbol{\Theta}_i}\left(\sum_{t=1}^{N}\frac{\partial^2 \mathbf{R}_b}{\partial \boldsymbol{\Theta}_1\partial \boldsymbol{\Theta}_t}\dot{\boldsymbol{\Theta}}_t\right)\cdots\right.$$

$$\left.\frac{\partial \mathbf{R}_b^T}{\partial \boldsymbol{\Theta}_i}\left(\sum_{t=1}^{N}\frac{\partial^2 \mathbf{R}_b}{\partial \boldsymbol{\Theta}_n\partial \boldsymbol{\Theta}_t}\dot{\boldsymbol{\Theta}}_t\right)\right]\dot{\boldsymbol{\Theta}}. \tag{B.5}$$

Now, the second part of kinetic energy is obtained:

$$T_b = \frac{1}{2}\boldsymbol{\omega}_b^T.\mathbf{I}_b.\boldsymbol{\omega}_b\frac{\partial T_b}{\partial \dot{\boldsymbol{\Theta}}_i} = \frac{\partial}{\partial \dot{\boldsymbol{\Theta}}_i}\left(\frac{1}{2}\boldsymbol{\omega}_b^T.\mathbf{I}_b.\boldsymbol{\omega}_b\right) =$$

$$\frac{1}{2}\left(\frac{\partial \boldsymbol{\omega}_b^T}{\partial \dot{\boldsymbol{\Theta}}_i}.\mathbf{I}_b.\boldsymbol{\omega}_b + \boldsymbol{\omega}_b^T.\mathbf{I}_b.\frac{\partial \boldsymbol{\omega}_b}{\partial \dot{\boldsymbol{\Theta}}_i}\right) = \boldsymbol{\omega}_b^T.\mathbf{I}_b.\frac{\partial \boldsymbol{\omega}_b}{\partial \dot{\boldsymbol{\Theta}}_i}$$

$$\frac{d}{dt}\left(\boldsymbol{\omega}_b^T.\mathbf{I}_b.\frac{\partial \boldsymbol{\omega}_b}{\partial \dot{\boldsymbol{\Theta}}_i}\right)$$

$$= \dot{\omega}_b^T.\mathbf{I}_b.\frac{\partial \boldsymbol{\omega}_b}{\partial \dot{\boldsymbol{\Theta}}_i} + \boldsymbol{\omega}_b^T.\mathbf{I}_b.\frac{d}{dt}\left(\frac{\partial \boldsymbol{\omega}_b}{\partial \dot{\boldsymbol{\Theta}}_i}\right) \tag{B.6}$$

On the other hand

$$\dot{\omega}_b = \sum_{s=1}^{N}\left(\frac{\partial \boldsymbol{\omega}_b}{\partial \boldsymbol{\Theta}_i}\dot{\boldsymbol{\Theta}}_s + \frac{\partial \boldsymbol{\omega}_b}{\partial \dot{\boldsymbol{\Theta}}_i}\ddot{\boldsymbol{\Theta}}_s\right), \tag{B.7}$$

and

$$\frac{d}{dt}\left(\frac{\partial \boldsymbol{\omega}_b}{\partial \dot{\boldsymbol{\Theta}}_i}\right) = \sum_{s=1}^{N}\frac{\partial^2 \boldsymbol{\omega}_b}{\partial \boldsymbol{\Theta}_s\partial \dot{\boldsymbol{\Theta}}_i}\boldsymbol{\Theta}_s. \tag{B.8}$$

Hence, it is found that:

$$\frac{\partial T_b}{\partial \boldsymbol{\Theta}_i} = \boldsymbol{\omega}_b.\mathbf{I}_b.\frac{\partial \boldsymbol{\omega}_b}{\partial \boldsymbol{\Theta}_i}. \tag{B.9}$$

Substituting Eqs. (B.8) and (B.9) into Eq. (B.6) and transforming them into matrix form, the next equation is derived:

$$\frac{d}{dt}\left(\frac{\partial T_b}{\partial \dot{\boldsymbol{\Theta}}_i}\right)-\frac{\partial T_b}{\partial \boldsymbol{\Theta}_i}$$
$$=\left[\frac{\partial \boldsymbol{\omega}_b}{\partial \boldsymbol{\Theta}_1}.\mathbf{I}_b.\frac{\partial \boldsymbol{\omega}_b}{\partial \dot{\boldsymbol{\Theta}}_i}\cdots\cdots\frac{\partial \boldsymbol{\omega}_b}{\partial \boldsymbol{\Theta}_n}.\mathbf{I}_b.\frac{\partial \boldsymbol{\omega}_b}{\partial \boldsymbol{\Theta}_i}\right]\dot{\boldsymbol{\Theta}}$$
$$+\left[\frac{\partial \boldsymbol{\omega}_b}{\partial \dot{\boldsymbol{\Theta}}_1}.\mathbf{I}_b.\frac{\partial \boldsymbol{\omega}_b}{\partial \dot{\boldsymbol{\Theta}}_i}\cdots\cdots\frac{\partial \boldsymbol{\omega}_b}{\partial \dot{\boldsymbol{\Theta}}_n}.\mathbf{I}_b.\frac{\partial \boldsymbol{\omega}_b}{\partial \dot{\boldsymbol{\Theta}}_i}\right]\ddot{\boldsymbol{\Theta}}$$
$$+\left[\boldsymbol{\omega}_b.\mathbf{I}_b.\frac{\partial^2 \boldsymbol{\omega}_b}{\partial \boldsymbol{\Theta}_1\partial \dot{\boldsymbol{\Theta}}_i}\cdots\cdots\boldsymbol{\omega}_b.\mathbf{I}_b.\frac{\partial^2 \boldsymbol{\omega}_b}{\partial \boldsymbol{\Theta}_n\partial \dot{\boldsymbol{\Theta}}_i}\right]$$
$$\dot{\boldsymbol{\Theta}}-\boldsymbol{\omega}_b.\mathbf{I}_b.\frac{\partial \boldsymbol{\omega}_b}{\partial \boldsymbol{\Theta}_i}. \tag{B.10}$$

Appendix C

Calculation of H, C and G.

$$\mathbf{H}_{ij}=m_b\frac{\partial \mathbf{R}_b^T}{\partial \boldsymbol{\Theta}_i}.\frac{\partial \mathbf{R}_b}{\partial \boldsymbol{\Theta}_j}+\frac{\partial \boldsymbol{\omega}_b^T}{\partial \dot{\boldsymbol{\Theta}}_i}$$
$$\mathbf{I}_b.\frac{\partial \boldsymbol{\omega}_b}{\partial \dot{\boldsymbol{\Theta}}_j}+\sum_{L=1}^{n}\left(J_r\frac{\partial \theta_{mL}^T}{\partial \boldsymbol{\Theta}_i}.\frac{\partial \theta_{mL}}{\partial \boldsymbol{\Theta}_j}\right)$$
$$+\sum_{L=1}^{n}\left\{m_w\left(\frac{\partial \rho_L^T}{\partial \boldsymbol{\Theta}_i}.\frac{\partial \rho_L}{\partial \boldsymbol{\Theta}_j}+\frac{\partial \eta_L^T}{\partial \boldsymbol{\Theta}_i}.\frac{\partial \eta_L}{\partial \boldsymbol{\Theta}_j}\right)\right.$$
$$\left.+I_{wy}\left(\frac{\partial \theta_L^T}{\partial \boldsymbol{\Theta}_i}.\frac{\partial \theta_L}{\partial \boldsymbol{\Theta}_j}\right)+I_{wz}\left(\frac{\partial \varphi^T}{\partial \boldsymbol{\Theta}_i}.\frac{\partial \varphi}{\partial \boldsymbol{\Theta}_j}\right)\right\}$$
$$+\sum_{L=1}^{n}\left\{m_L\frac{\partial h_L^T}{\partial \boldsymbol{\Theta}_i}.\frac{\partial h_L}{\partial \boldsymbol{\Theta}_j}+\frac{\partial \mathbf{W}_L^T}{\partial \dot{\boldsymbol{\Theta}}_n}.m_L.\frac{\partial \mathbf{W}_L}{\partial \dot{\boldsymbol{\Theta}}_i}\right.$$
$$\left.+\frac{1}{2}m_L\frac{\partial \mathbf{W}_L^T}{\partial \boldsymbol{\Theta}_i}.\frac{\partial h_L}{\partial \boldsymbol{\Theta}_n}\right\}. \tag{C.1}$$

The presented matrix C is composed of two parts, including $\mathbf{C}_{1ij}$ representing terms with $\dot{\boldsymbol{\Theta}}$ coefficients, and representing terms that are not coefficients of $\dot{\boldsymbol{\Theta}}$. Accordingly, the matrix C is defined as:

$$\mathbf{C}=\mathbf{C}_{1ij}\dot{\boldsymbol{\Theta}}+\mathbf{C}_{2i}, \tag{C.2}$$

where,

$$\mathbf{C}_{1ij}=\left(\mathbf{C}_1\frac{\partial \boldsymbol{\delta}^T{}_1}{\partial \boldsymbol{\Theta}_i}.\frac{\partial \boldsymbol{\delta}_1}{\partial \boldsymbol{\Theta}_j}+\mathbf{C}_2\frac{\partial \boldsymbol{\delta}_2^T}{\partial \boldsymbol{\Theta}_i}.\frac{\partial \boldsymbol{\delta}_2}{\partial \boldsymbol{\Theta}_j}+\cdots\right)$$
$$+m_b\frac{\partial \mathbf{R}_b^T}{\partial \boldsymbol{\Theta}_i}.\left(\sum_{s=1}^{N}\frac{\partial^2 \mathbf{R}_b}{\partial \boldsymbol{\Theta}_s\partial \boldsymbol{\Theta}_j}\right)$$
$$+\frac{\partial \boldsymbol{\omega}_b^T}{\partial \dot{\boldsymbol{\Theta}}_i}.\mathbf{I}_b.\frac{\partial \boldsymbol{\omega}_b}{\partial \boldsymbol{\Theta}_j}+{\boldsymbol{\omega}_b}^T.\mathbf{I}_b.$$
$$\frac{\partial^2 \boldsymbol{\omega}_b}{\partial \dot{\boldsymbol{\Theta}}_i\partial \boldsymbol{\Theta}_j}+J_r\frac{\partial \theta_{m1}^T}{\partial \boldsymbol{\Theta}_i}.$$
$$\left(\sum_{s=1}^{N}\frac{\partial^2 \theta_{m1}}{\partial \boldsymbol{\Theta}_s\partial \boldsymbol{\Theta}_j}+\cdots\right)$$
$$+m_w\left(\frac{\partial \rho_1^T}{\partial \boldsymbol{\Theta}_i}.\left(\sum_{s=1}^{N}\frac{\partial^2 \rho_1}{\partial \boldsymbol{\Theta}_s\partial \boldsymbol{\Theta}_j}\right)\right.$$
$$\left.+\cdots+\frac{\partial \eta_1^T}{\partial \boldsymbol{\Theta}_i}.\left(\sum_{s=1}^{N}\frac{\partial^2 \eta_1}{\partial \boldsymbol{\Theta}_s\partial \boldsymbol{\Theta}_j}\right)+\cdots\right)$$
$$+I_{wy}\left(\frac{\partial \theta_1^T}{\partial \boldsymbol{\Theta}_i}.\left(\sum_{s=1}^{N}\frac{\partial^2 \theta_1}{\partial \boldsymbol{\Theta}_s\partial \boldsymbol{\Theta}_j}\right)+\cdots\right)$$
$$+I_{wz}\frac{\partial \varphi^T}{\partial \boldsymbol{\Theta}_i}.\left(\sum_{s=1}^{N}\frac{\partial^2 \varphi}{\partial \boldsymbol{\Theta}_s\partial \boldsymbol{\Theta}_j}\right)$$
$$+\sum_{L=1}^{n}\left\{m_L\frac{\partial h_L^T}{\partial \boldsymbol{\Theta}_i}.\left(\sum_{t=1}^{N}\frac{\partial^2 h_L}{\partial \boldsymbol{\Theta}_n\partial \boldsymbol{\Theta}_t}\right)\right.$$
$$\left.+\frac{\partial \mathbf{W}_L^T}{\partial \boldsymbol{\Theta}_n}.m_L.\frac{\partial \mathbf{W}_L}{\partial \dot{\boldsymbol{\Theta}}_i}+{\mathbf{W}_L}^T.m_L.\frac{\partial^2 \mathbf{W}_L}{\partial \boldsymbol{\Theta}_n\partial \dot{\boldsymbol{\Theta}}_i}\right\}$$
$$+\sum_{L=1}^{n}\left\{\frac{1}{2}m_L\frac{\partial h_L^T}{\partial \boldsymbol{\Theta}_i}.\frac{\partial \mathbf{W}_L}{\partial \boldsymbol{\Theta}_n}+\frac{1}{2}m_L\right.$$
$$\left.\frac{\partial \mathbf{W}_L^T}{\partial \boldsymbol{\Theta}_i}.\left(\sum_{t=1}^{N}\frac{\partial^2 h_L}{\partial \boldsymbol{\Theta}_n\partial \boldsymbol{\Theta}_t}\right)\right\}. \tag{C.3}$$

Moreover, the matrices $\mathbf{C}_{2i}$ and G_i are written as:

$$\mathbf{C}_{2i}=-\left({\boldsymbol{\omega}_b}^T.\mathbf{I}_b.\frac{\partial \boldsymbol{\omega}_b}{\partial \boldsymbol{\Theta}_i}\right)-\sum_{L=1}^{n}{\mathbf{W}_L}^T.m_L.\frac{\partial \mathbf{W}_L}{\partial \boldsymbol{\Theta}_i}, \tag{C.4}$$

$$G_i=\left(K_1\boldsymbol{\delta}_1.\frac{\partial \boldsymbol{\delta}_1}{\partial \boldsymbol{\Theta}_i}+\cdots\right)+m_b\mathbf{g}^T\frac{\partial \mathbf{R}_b}{\partial \boldsymbol{\Theta}_i}+\frac{1}{2}K_1^t$$
$$\left(2\theta_1\frac{\partial \theta_1}{\partial \boldsymbol{\Theta}_i}+2\theta_{m1}\frac{\partial \theta_{m1}}{\partial \boldsymbol{\Theta}_i}-2\frac{\partial \theta_1}{\partial \boldsymbol{\Theta}_i}\theta_{m1}\right.$$
$$\left.-2\frac{\partial \theta_{m1}}{\partial \boldsymbol{\Theta}_i}\theta_1\right)+\cdots. \tag{C.5}$$

Biographies

Moharam Habibnejad Korayem received his BSc (Hon) and MSc in Mechanical Engineering from the Amirkabir University of Technology in 1985 and 1987, respectively. He obtained his PhD degree in mechanical engineering from the University of Wollongong,

Australia, in 1994. He is a Professor of mechanical engineering at the Iran University of Science and Technology. He has been involved with teaching and research activities in the robotics areas at the Iran University of Science and Technology for the last 19 years. His research interests include dynamics of elastic mechanical manipulators, trajectory optimization, symbolic modeling, robotic multimedia software, mobile robots, industrial robotics standard, robot vision, soccer robot, and the analysis of mechanical manipulators with maximum load-carrying capacity. He has published more than 550 papers in international journals and conferences in the robotic area.

Siavash Fathollahi Dehkordi received his BSc and MSc in Mechanical Engineering from the Iran University of Science and Technology. His MSc thesis engaged him with robotics and especially dynamic modeling, new robot structures, and control in this field. The areas were so attractive that they led him towards a PhD in robotics and multi-body system dynamics. He received his PhD in October 2018 from the School of Mechanical Engineering, Iran University of Science and Technology. In 2019, he joined the mechanical engineering department at Shahid Chamran University of Ahvaz as an Assistant Professor. His research interests include Robotics, Mechatronics, Multi-body system dynamics, Nonlinear dynamic analysis, Mobile robots, and Flexible manipulators.

Mostafa Aghajari earned his MSc in Mechanical Engineering from the Iran University of Science and Technology. His MSc thesis engaged him with robotics and especially dynamic modeling, new robot structures, and control in this field. His research interests include Robotics, Mechatronics, Multi-body system dynamics, Nonlinear dynamic analysis, Mobile robots, and Flexible manipulators.